



**HAL**  
open science

# Contrast resolution enhancement of Ultrasonic Computed Tomography using a wavelet-based method – Preliminary results in bone imaging

Philippe Lasaygues, Régine Guillermin, Khaled Metwally, Samantha Fernandez, Laure Balasse, Philippe Petit, Cécile Baron

## ► To cite this version:

Philippe Lasaygues, Régine Guillermin, Khaled Metwally, Samantha Fernandez, Laure Balasse, et al.. Contrast resolution enhancement of Ultrasonic Computed Tomography using a wavelet-based method – Preliminary results in bone imaging. International Workshop on Medical Ultrasound Tomography, Nov 2017, Speyer, Germany. hal-01769818

**HAL Id: hal-01769818**

**<https://hal.science/hal-01769818>**

Submitted on 18 Apr 2018

**HAL** is a multi-disciplinary open access archive for the deposit and dissemination of scientific research documents, whether they are published or not. The documents may come from teaching and research institutions in France or abroad, or from public or private research centers.

L'archive ouverte pluridisciplinaire **HAL**, est destinée au dépôt et à la diffusion de documents scientifiques de niveau recherche, publiés ou non, émanant des établissements d'enseignement et de recherche français ou étrangers, des laboratoires publics ou privés.

# **Contrast resolution enhancement of Ultrasonic Computed Tomography using a wavelet-based method – Preliminary results in bone imaging**

Philippe Lasaygues<sup>1</sup>, Régine Guillermin<sup>1</sup>, Khaled Metwally<sup>1</sup>, Samantha Fernandez<sup>2</sup>, Laure Balasse<sup>2,3</sup>, Philippe Petit<sup>4</sup>, Cécile Baron<sup>5</sup>

<sup>1</sup> Aix Marseille Univ, CNRS, Centrale Marseille, LMA, Marseille, France

E-mail: lasaygues@lma.cnrs-mrs.fr

<sup>2</sup> Aix-Marseille Univ, CERIMED, Marseille, France

<sup>3</sup> Aix Marseille Univ, INSERM, VRCM, Marseille, France

<sup>4</sup> Dep. of Pediatric and Prenatal Radiol., "Timone" Children-Hospital, APHM, Marseille, France

<sup>5</sup> Aix Marseille Univ, CNRS, ISM, Marseille, France

## **Abstract**

Ultrasonic Computed Tomography (USCT) is a biological tissue imaging modality. USCT is mainly efficient in improving image resolution by eliminating noise and interferences. The strong variations in acoustic properties between soft tissues and bone generate complex signals consisting of several packets with different signatures. USCT contrast ratio is degraded. In this paper, a method to enhance USCT resolution is investigated. The method, called the "Wavelet-based Coded Excitation" (WCE) method, is based on the wavelet decomposition of the signal and on a suitable transmitted incident wave correlated with the experimental set-up, mathematically expressed using an extended form of simulated annealing. The goal of this study is to investigate the feasibility of the WCE method to enhance the Contrast-to-Noise Ratio of USCT for bone objects. Experiments are conducted with a bone phantom, and with a chicken drumstick, using a circular antenna equipped with 1MHz-transducers. Results demonstrate the capabilities and limitations of the method.

**Keywords:** ultrasonic tomography, resolution, coded-excitation, wavelet, bone

## **1 Introduction**

Currently, X-ray Tomography offers significant advantages for the measurement of Bone Mineral Density (BMD). However, the limited spatial resolution of some today's devices makes an accurate measurement of cortical thickness difficult to obtain, and an assessment of

cortical density almost impossible [1]. As a consequence, published data concerning cortical density should be reviewed carefully. For example, cortical density measurement limitations were confirmed in children and newborns. Significant correlations of total radius cross-sectional area, cortical area and cortical thickness with weight and height were found but with no gender differences [2]. Nevertheless, BMD remains today the “gold-standard” parameter, reporting essentially on the bone mineral contents. It is also worth noting that BMD does not describe the micro-architecture of bone, and that the ultrasonic waves are successfully used to determine other parameters than density, such as elasticity or porosity [3], [4]. X-ray (and also Magnetic Resonance Imaging-MRI) modalities are associated with different constraints and inconveniences (worse in the case of pediatric application), according to the type of examination: cost, radiation, sedation, availability, and accessibility, while Ultrasound is a non-invasive, non-irradiant, and painless modality. Ultrasound scanners are little expensive (compared to X-ray or MRI scanners) and can be used at the patient bedside. However, ultrasound has difficulty penetrating bone and, therefore, can only detect the outer surface of bony structures and not what lies within it. In current medical practice, the sub-cortical imaging is not possible, and no information on the cortical thickness and the medullar underlying tissue is available. The physical distribution of cortical bone within the measured site may influence acoustical measurements, and thus the electro-acoustical setup may not be adapted in terms of signal processing, amplification, or gain. Furthermore, the map is a bi-dimensional representation of the impedance variation between soft and hard tissues, but is not parametrical (the gray level set is not related to the value). And when a periosteal reaction occurs on adjacent bones (ribs, tibia-fibula), the resolution of echographic images may be limited, especially between the two bones. There are also limitations to the depth that sound waves can penetrate; therefore, deeper structures in larger or fatter patients may not be seen easily. For visualizing internal structure of bones or certain joints, others imaging modalities are used.

Ultrasonic Computed Tomography (USCT), a numerical two dimensional (2D) data inversion method, appears to be a possible alternative in view of the limits of medical sonography, making it possible, on one hand, to take into account the physical phenomena due to wave propagation in hard tissues, with appropriate modeling, and, on the other hand, to reach one or more significant parameters of the structure like the speed of sound or attenuation. Based on the linearization of the inverse problem of acoustic wave propagation, USCT generates cross-sectional images of biological soft tissues [5]–[7]. Difficulties occur in hard tissue imaging [7], due to the great differences between tissue impedance, and to the high echogenic index of the bone, which strongly alters the propagation of the ultrasonic waves, and generally induces low contrast resolution, and low Contrast-to-Noise Ratio (CNR). The physical phenomena associated with wave propagation make it necessary to modify the methods used for the acquisition of the ultrasonic signals. The use of low ultrasound frequencies ( $\leq 3\text{MHz}$ ) provides an effective possible solution [8]. However, if the depth of the field increases, the resolution of the signals and hence that of the reconstructed images is

bound to decrease. Even with low frequencies, the wave propagation process generates extremely complex acoustic signals, which are often difficult to interpret in terms of wave path, volume, guided or surface waves, and attenuation. To improve the quality of the signals, focus should be placed on signal processing such as filtering, spectrum analysis and method involving the deconvolution of the signals using a characteristic transfer function of the experimental device [9]. Deconvolution algorithms increase the bandwidth of the frequency spectrum, but they tend to be over unstable and prone to noise. Loosvelt and Lasaygues [10] developed an alternative method based on a multi-scale signal decomposition procedure, making it possible to process all the information available in terms of frequency and time. This method, called the "Wavelet-based Coded Excitation" (WCE) method, was used to determine, independently, the velocity of the ultrasonic wave and the wave path across the thickness of a 1D-parallelepiped plate. The aim of this new study is to investigate the feasibility of the WCE method as a means of CNR enhancement of bone imaging. In this two-dimensional case, the wavelet decomposition alone does not suffice to optimize the signal processing, and the incident wave reaching the object also should match the wavelets' mathematical properties. We thus propose a solution to achieve this goal, based on a zone-by-zone simulated annealing algorithm. Then, we show the usefulness of the WCE method through experimental results on a human bone (without soft tissues) mimicking phantom, and on an *ex vivo* chicken drumstick (without skin).

## 2 Material and method

### 2.1 USCT statements

By now, basic USCT principles have been clearly established in the case of weakly varying media such as low-contrast structures, i.e., almost homogeneous media [5], [6], [11]. A constant reference medium can therefore be chosen and approximations will be made over an unperturbed background. The scattering problem can be linearized by using the first-order Born approximation, and if the Green's function of the unperturbed problem (the background) is known, the forward problem can be solved with the Lippmann-Schwinger integral equation. A method to solve this inverse problem will consist in performing a far field asymptotic development. The USCT algorithm will yield the perturbation with respect to the reference problem. This leads to a linear relation between the object function (or contrast function) and the scattered field, particularly in the far-field (2D Fourier transform) case, which makes it possible to reconstruct the object function in almost real time, based on a sufficiently large set of scattering data. The details of the algorithm used in this work can be found in [12], [13]. In the case of hard biological tissues having larger acoustical impedances than those of the surrounding medium, the weak scattering hypothesis is not realistic. Nevertheless, if the imaging objective involves parameters such as the bone thickness, the problem can be viewed as how to identify a water-like cavity (the object) located in an elastic cylinder

immersed in a water-like fluid. In this configuration, one solution consists in using the low frequency ultrasonic wave propagation scheme, because the penetration length of the wave will be greater than a high frequency scheme, and the Born approximation will still be satisfied. The background can be defined in terms of the solid part without any hole, surrounded by water, and the perturbation, i.e., the object to be reconstructed, would be the cavity. Image reconstruction can then be performed by means of an efficient back-projection method implemented using standard graphics algorithms [8].

## 2.2 USCT device and calibration

An USCT device prototype has been developed by our laboratory (Figure 1).

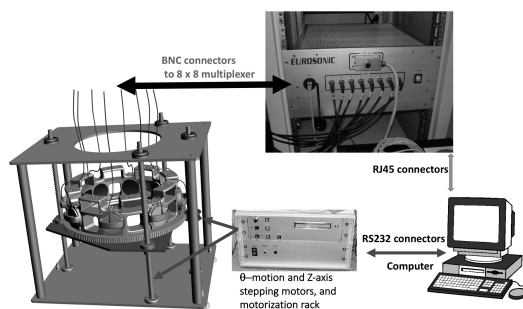


Figure 1: Photo and design drawing of the device and setup.

The device consists of a multiplexed 2D-ring antenna. The crown of the antenna has an inner radius of 150 mm and supports 8 fixed transducers distributed over  $360^\circ$  ( $\Delta\theta = 45^\circ$ ). The object to be imaged is positioned in the hypothetical geometrical center of the ring. By means of stepping motors and of an electronic motorization rack to manage the mechanical movements, the crown can turn  $45^\circ$  degrees in  $1/100$  degree increments of and move vertically for multiple image slicing (limit stroke 200mm). For a given height, it is thus possible to acquire sinograms with 64 projections (8 transmitters x 8 receivers). Then, signals from every rotation (32 in this work) are used to get a complete sinogram with  $64 \cdot 32 = 2048$  signals, and a combination according to the angles of diffraction. Thus, we simulate an antenna comprising a greater number of emitters and receivers. The scattered pressure field is obtained by subtracting the total pressure field (measured in the presence of the object) and the incident pressure field (measured in the absence of the object). Experimentally, this consists in eliminating the data from the direct transmission between transducers facing each other with their axes aligned. The Mistras-Eurosonic™ multiplexer equipped with an 8-by-8 parallel-channel acquisition system allows the formation of arbitrary waveforms and beam-forming over 8 independent channels. Transmitted and received ultrasonic radio-frequency (RF-)signals are digitized (4096 samples by signal, resolution of 12 bits, sampling frequency of 20 MHz). The power amplifier gives a variable output voltage from 10 mV to 50 mV. The

8 transducers are Imasonic™ piezo-composite transducers with a center frequency of 1 MHz, and the -6 dB bandwidth is 1.46 MHz (from 0.48 MHz to 1.95 MHz). They are equally spaced (every 45°) on the crown. Each transducer is 60 mm high and 56 mm in diameter. These transducers have a focal length of 150 mm in the Fresnel zone, a lateral aperture size of 40 mm and an axial aperture size of 30 mm. The slice thickness is 3 mm. The mean center frequency is 1.08 MHz ± 0.1 MHz. Fluctuations in the position of the transducers on the crown can give rise to time-shift variations which degrade the spatial resolution of the USCT. Here to assess these biases, a 70µm-diameter copper thread is placed in the center of the crown. For each signal, the correction process is a temporal offset between the signal and the reference signal obtained at the same angle on the thread sinogram (Point Spread Function-PSF of the device).

### 2.3 Pulse-mode method

The electro-acoustic device and the transducers therefore serve as a continuous, linear, stationary causal filter (Figure 2).

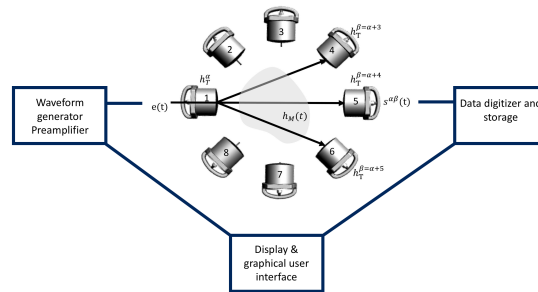


Figure 2: Electro-acoustical synoptic of the 8-parallel-channel acquisition system

The transmitted  $x^{\alpha\beta}(t)$  and received  $s^{\alpha\beta}(t)$  signals are connected by convolution:

$$\text{Eq. 1} \quad s^{\alpha\beta}(t) = x^{\alpha\beta}(t) \otimes h_M(t)$$

$$\text{Eq. 2} \quad x^{\alpha\beta}(t) = (h_T^\alpha \otimes h_T^\beta \otimes e)(t)$$

where  $\otimes$  denotes the convolution operation;  $e(t)$  is the electrical input conveyed to the transducer via the waveform generator;  $h_T^\alpha$  and  $h_T^\beta$  are the responses of the electro-acoustic device including the waveform generator, multiplexer and transducers no  $\alpha$  and no  $\beta$  ( $\alpha = \beta = [1, \dots, 8]$ ), respectively, of the circular antenna in diffraction mode;  $h_M(t)$  is the response of the object under investigation. At this stage, the responses of the 8 transducers are supposed identical. Here, the choice of the electrical input  $e(t)$  (independently for each pulse- or wavelet-mode method) is made on the total transmitted field in the absence of the object. The measurement is carried out in transmission between two opposite and aligned transducers ( $\alpha = [1, \dots, 8]$ ;  $\beta = \alpha + 4$ ). Then, in the absence of any object, the transmitted response,  $h_M(t)$ , in water depends on the time delay of the wave - which is proportional

to the distance  $d^{\alpha\beta}$  between one transmitter ( $\alpha = [1, \dots, 8]$ ) and one receiver ( $\beta = \alpha + 4$ ) - and on its velocity  $v_0$ . The initial output signal,  $[s^{\alpha\beta}(t)]^{init}$ , is therefore equal to the input signal  $x^{\alpha\beta}(t)$ , which is invariant by translation:

$$\text{Eq. 3: } [s^{\alpha\beta}(t)]^{init} = x^{\alpha\beta}(t) \otimes \delta\left(t - d^{\alpha\beta}/v_0\right) = x^{\alpha\beta}(t)$$

Here, to obtain control experimental data, USCT is first realized using a conventional ultrasonic pulse-mode method. The electrical input signal  $e(t)$  was a pulse signal, which was comparable to a Dirac delta function (in terms of the distribution), and  $[s^{\alpha\beta}(t)]^{init}$  is given by

$$\text{Eq. 4: } [s^{\alpha\beta}(t)]^{init} = (h_T^\alpha \otimes h_T^\beta)(t)$$

## 2.4 Wavelet-based coded excitation (WCE) method

Based on the orthogonal wavelet decomposition of the signal, it is possible to obtain a time versus scale diagram, giving the evolution of the frequencies with time. Like time-scale processing, wavelet decomposition lends itself very well to detecting and discriminating between signals during the data pre-processing phase as well as during the filtering step of an image reconstruction phase. If the initial received signal  $x^{\alpha\beta}(t)$  is a wavelet denoted  $\varphi_j(t)$ , centered on the scale  $J$  ( $j \in \mathbb{Z}$ ) and with suitable properties for specific wavelet analysis, previously analyzed by Y. Meyer and S. Jaffard [14], [15], Eq. 1 can be written:

$$\text{Eq. 5 } s^{\alpha\beta}(t) = (\varphi_j \otimes h_M)(t)$$

The coded-excitation method is thus based on a time-scale decomposition of the signal  $s^{\alpha\beta}(t)$  giving the suitable coefficients  $X_j^{\alpha\beta}(t)$ :

$$\text{Eq. 6 } X_j^{\alpha\beta}(t) = \langle s^{\alpha\beta}(t), \phi_j(t) \rangle = h_M(t) \otimes [\varphi_j \otimes \phi_j](t)$$

where  $\phi_j$  is a wavelet centered on the scale  $j$  ( $j \in \mathbb{Z}$ ). The properties of the wavelet decomposition, an orthogonal decomposition in this case, are such that the coefficients  $X_j^{\alpha\beta}(t)$  nullify everywhere except for  $j = J$  (the details of the algorithm can be found in [10]).

## 2.5 Acoustical modeling

As detailed in [12], reconstruction is performed using the summation of filtered back-projections" algorithm. Each pixel of the image corresponds to a coordinate of a point corresponding to a transmitter-receiver pair, that is to say, for each recorded signal. The coordinates of the point in the sinogram are the signal number (ordinate) and the time of flight (abscissa). The time of flight for each pair of transducers must be accurately measured. The working hypothesis adopted in this study is that, depending on the angle of observation, the object is comparable to a bilayer composed of two parallelepiped plates. The ultrasonic incident wave vector is perpendicular to the water/object interface. The object is taken to be

homogeneous and isotropic. The first-arriving signals are assumed to be the signals from the water/bone interface and the last arriving signals are assumed to be the compressional wave propagating off the back wall. Three configurations are taken into account for this modeling: reflection (transducers  $\alpha - \alpha$ ), back-propagation (couple of transducers  $\alpha - \alpha + 1$  and  $\alpha - \alpha + 7$ ), and diffraction (couple of transducers  $\alpha - \alpha + 2$ ,  $\alpha - \alpha + 3$ ,  $\alpha - \alpha + 5$ ,  $\alpha - \alpha + 6$ ). In the transmission mode, the directly transmitted wave field signals are eliminated. Only the echo mode is considered for the first and second configuration, and only the transmission mode for the third configuration. All the other phenomena (shear waves, guided waves, etc.) are insignificant or will occur too late to affect the compressional wave processes. Therefore, the received signal can be modeled as the sum of several wave packets.  $h_M(t)$  is comparable to a sum of Dirac delta functions.

$$\text{Eq. 7} \quad s^{\alpha\beta}(t) = A_1^{\alpha\beta} \varphi_j(t - t_1^{\alpha\beta}) + A_2^{\alpha\beta} \varphi_j(t - t_2^{\alpha\beta}) + \dots + A_n^{\alpha\beta} \varphi_j(t - t_n^{\alpha\beta})$$

$A_n^{\alpha\beta}$  are the amplitudes of the wave packets located at  $t_n^{\alpha\beta}$  between transducers  $\text{no}\alpha$  and  $\text{no}\beta$ . As indicated by Loosvelt and Lasaygues [10],  $t_n^{\alpha\beta}$  can be measured by cross-correlation between the signal received  $s^{\alpha\beta}(t)$  and a predetermined analyzing pattern. The result is the sum of the functions  $X_j^{\alpha\beta}(t)$ . The locations of times  $t_n^{\alpha\beta}$  correspond to the signals from the object's inner structure.

$$\text{Eq. 8:} \quad X_j^{\alpha\beta}(t) = A_1^{\alpha\beta} \langle \varphi_j(t - t_1^{\alpha\beta}), \phi_j(t) \rangle + A_2^{\alpha\beta} \langle \varphi_j(t - t_2^{\alpha\beta}), \phi_j(t) \rangle + \dots + A_n^{\alpha\beta} \langle \varphi_j(t - t_n^{\alpha\beta}), \phi_j(t) \rangle$$

$$\text{Eq. 9:} \quad X_j^{\alpha\beta}(t) = X_j^{\alpha\beta}(t - t_1^{\alpha\beta}) + X_j^{\alpha\beta}(t - t_2^{\alpha\beta}) + \dots + X_j^{\alpha\beta}(t - t_n^{\alpha\beta})$$

If it is possible to process the initial signal received  $X^{\alpha\beta}(t)$  in such a way that it is identical to a wavelet function, this method then yields the parameters of interest without any further filtering effects being involved. The main problem is how to digitize an initial electric input signal  $e(t)$  in order to obtain  $x^{\alpha\beta}(t) = \varphi_j(t)$ .

## 2.6 Wavelet form

In the 1D-transmission mode, Loosvelt and Lasaygues [10] previously performed direct spectral Wiener deconvolution between the wavelet  $\varphi_j(t)$  and the received signal that was recorded when the electrical input signal  $e(t)$  was a Dirac delta function. In the 2D-mode measurements, although the signals mostly overlapped, considerable differences between the theoretical wavelets and those actually generated using the same algorithm and the same center frequency were observed between the transducers in diffraction mode (couple of transducers  $(\alpha - \alpha + 2)$ ,  $(\alpha - \alpha + 3)$ ,  $(\alpha - \alpha + 5)$ ,  $(\alpha - \alpha + 6)$ ). Conil et al. [16] uses a non-linear scheme and a simulated annealing algorithm [17]. The advantage of the method is that it is not necessary to know the response of the system to find a suitable input signal. This involves iteratively testing many input signals and analyzing the corresponding output

signals. During the search, the probability of finding an input signal is defined as a function of the deviation between the output signal obtained and the sought signal.

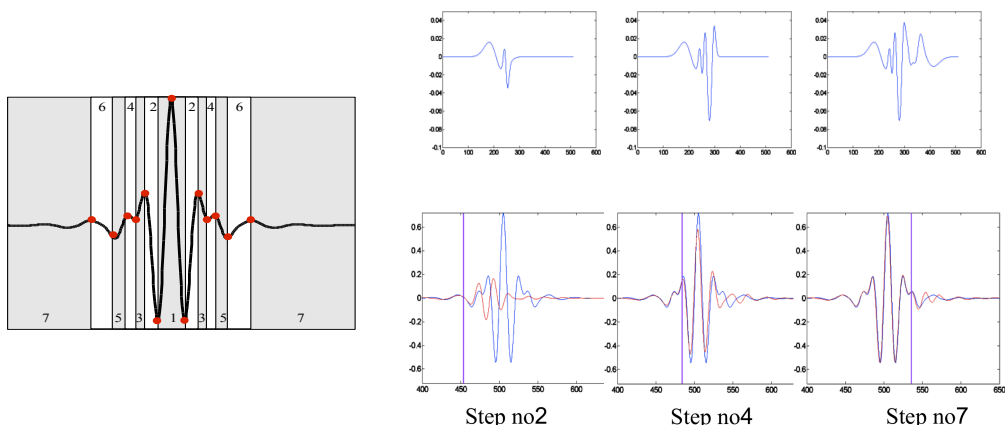


Figure 3: (left) Wavelet form (S. Jaffard function [18]) with  $J = -4$ , matching zones delimited by local extrema. (right) Illustration of 3 steps of the construction of the wavelet ( $J = -4$ ) by simulated annealing. (top) input signal  $e(t)$ , (bottom) reconstructed signal

This probability is extended to zero; the more slowly the function tends towards zero, the better the result. Here, to limit the number of signals to be tested, which can be very important, and very time-consuming, the algorithm is adapted to the wavelet, which corresponds to the bandwidth of the 1 MHz-transducer (center frequency 0.83 MHz, bandwidth [0.42 MHz – 1.66 MHz], corresponding to  $J = -4$ ) (Figure 4). This wavelet contains several local extrema (Figure 3), and the simulated annealing algorithm is applied zone by zone - the zones being delimited by local extrema. Because the wavelet is symmetrical, the number of matching zones is reduced, and the process extends iteratively from left to right of the targeted waveform (Figure 3).

The algorithm includes 8 iterations. For each step, the atoms (main functions calculating during the simulated annealing algorithm) are determined one after the other. Once all the atoms are defined, all their parameters are adjusted to obtain the best output signal.

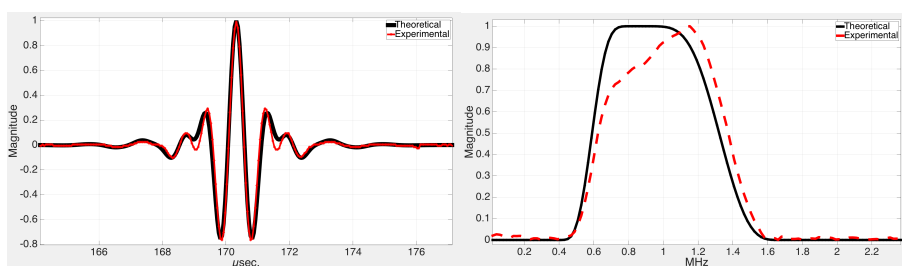


Figure 4: Time (left) and spectral (right) graph of the theoretical (black line) and the experimental (red dash line) wavelet between transmitter  $n^{\circ}1$  and receiver  $n^{\circ}4$  ( $\theta = 135^{\circ}$ ) in the absence of any object

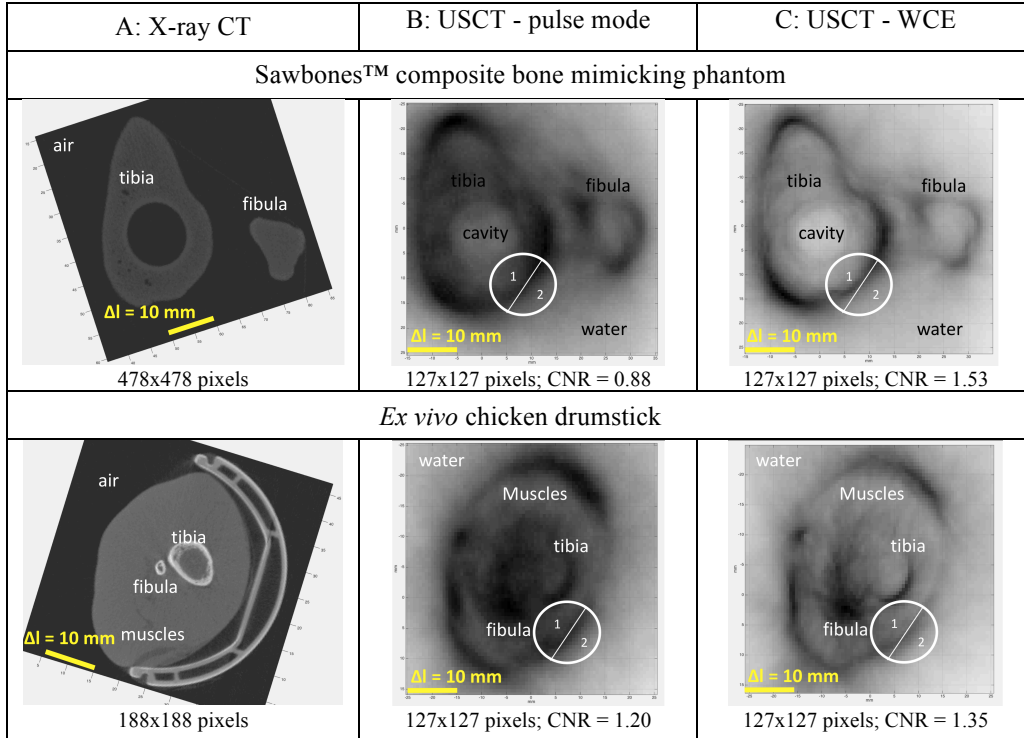


Figure 5: X-ray CT (A), USCT using an electric pulse (B), and wavelet  $\varphi_{-4}(t)$  (C), of a Sawbones™ composite bone mimicking phantom (top) and an *ex vivo* chicken drumstick without skin (bottom). The white circle represents the regions involved in Contrast-to-Noise Ratio calculation.

### 3 Results

Experiments were conducted to confirm the performance of the developed method. Two objects were analyzed. One human bone mimicking phantom (Sawbones™, tibia-fibula), and one *ex vivo* chicken drumstick without skin were studied. The cavity diameter of the tibia mimicking phantom was 12.5 mm, and its overall length 42 cm, and the fibula mimicking phantom had no inner cavity. The distance between bones ( $\sim 8$  mm) was measured using a caliper. The objects were set in water at room temperature prior to the experiments. The water tank temperature was  $21^{\circ}7$  and the ultrasonic wave velocity in water was 1486 m/s. USCT images of objects were compared with X-ray computed tomography (X-ray CT) images obtained at the same cross-section levels, with a nanoScan® PET/CT preclinical imager (Mediso™, Hungary). The slice thickness for the X-ray cross-section was 1.5 mm and the number of projections was 360. Cross-sections were chosen in the cortical areas of the bones; 100 mm from the proximal epiphysis for the bone phantom; and 25 mm for the chicken drumstick. The 2D-ultrasonic tomograms were obtained from two excitation modes:

the pulse excitation mode used an electric pulse as the input signal (Figure 5-B), while the WCE method used a signal corresponding to the wavelet  $\varphi_{-4}$  (Figure 5-C). The parameter commonly adopted to determine the quality of ultrasonic tomographic reconstructions is the Contrast-to-Noise Ratio (CNR) [19][20]. This criterion defines the contrast between two adjacent media as:

$$\text{Eq. 10} \quad \text{CNR}_{1,2} = \frac{|\overline{D}_1 - \overline{D}_2|}{\sqrt{\sigma_1^2 + \sigma_2^2}}$$

$\overline{D}_1$  and  $\overline{D}_2$  are the mean pixel values in regions 1 and 2, and  $\sigma_1$  and  $\sigma_2$  are the corresponding standard deviations. Both regions contain the same number of pixels. The object (region no1) contrast is assessed in comparison with the background (region no2). As CNR increases, noise decreases and quality increases.

## 4 Conclusion

The resolution of images obtained by USCT is not as good as that of images obtained by X-ray Computed Tomography. It was nevertheless possible to observe qualitatively the tibia and fibula cortical shells on the USCT-images for both phantom and chicken samples. When the WCE method was applied to USCT, a 42.5% increase in contrast was observed for the phantom object. The diameter of the inner cavity was found to be in the 11-13 mm range, which is close to the actual value of 12.5 mm. The external distance between tibia and fibula was found to be in the 5-7 mm range, rather far from the actual value (8mm). For the chicken drumstick, the contrast increased by 11%. The differentiation between tibia and fibula was more difficult. The image of the tibia was not complete, and its diameter could not be measured. The image of the fibula was not well resolved, and the distance between the two bones could not be measured. By applying the WCE method, the definition of the outer and inner boundaries of each bone was obtained with a much better contrast resolution than when using the electric pulse. The boundaries of the tibia were retrieved but the quality of this reconstruction was not satisfactory; the inner structure of the tibia was not resolved. To conclude, by applying the WCE method to cortical bone USCT, boundary imaging resolution was enhanced, even though sizes were different from the actual sizes.

**Acknowledgements:** This research was supported by the ANR funds, under Grant No. 11-BS09-032. The authors are grateful to Eric Debieu and Vincent Long at the Laboratory of Mechanics and Acoustics, (LMA) for their help in setting up experiments. The authors also thank Eduardo Morais Carvalho at Aix-Marseille University and Gladys Leger, at Centrale Marseille for their internship work.

## References

- [1] P. Augat, T. Link, T. F. Lang, J. C. Lin, S. Majumdar, and H. K. Genant, "Anisotropy of the elastic modulus of trabecular bone specimens from different anatomical locations," *Med. Eng. Phys.*, vol. 20, no. 2, pp. 124–131, Mar. 1998.
- [2] T. L. Binkley, R. Berry, and B. L. Specker, "Methods for measurement of pediatric bone," *Rev. Endocr. Metab. Disord.*, vol. 9, no. 2, pp. 95–106, Jun. 2008.
- [3] C. Baron, M. Talmant, and P. Laugier, "Effect of porosity on effective diagonal stiffness coefficients (cii) and elastic anisotropy of cortical bone at 1MHz: A finite-difference time domain study," *J. Acoust. Soc. Am.*, vol. 122, no. 3, pp. 1810–1817, Sep. 2007.
- [4] P. Laugier and G. Häät, *Bone quantitative ultrasound*. Dordrecht; New York: Springer Science, 2011.
- [5] N. V. Ruiter, T. O. Müller, R. Stotzka, and H. Gemmeke, "Evaluation of Different Approaches for Transmission Tomography in Ultrasound Computer Tomography," in *Bildverarbeitung für die Medizin 2005*, H.-P. Meinzer, H. Handels, A. Horsch, and T. Tolxdorff, Eds. Berlin/Heidelberg: Springer-Verlag, 2005, pp. 430–434.
- [6] N. Duric *et al.*, "Detection of breast cancer with ultrasound tomography: First results with the Computed Ultrasound Risk Evaluation (CURE) prototype: Detection of breast cancer with ultrasound tomography," *Med. Phys.*, vol. 34, no. 2, pp. 773–785, Jan. 2007.
- [7] P. Lasaygues, S. Mensah, R. Guillermin, J. Rouyer, and E. Franceschini, "Nonlinear inversion modeling for ultrasonic computed tomography: transition from soft to hard tissues imaging," in *Proceedings of SPIE*, 2012, vol. 8320, p. 832004.
- [8] P. Lasaygues, "Assessing the cortical thickness of long bone shafts in children, using two-dimensional ultrasonic diffraction tomography," *Ultrasound Med. Biol.*, vol. 32, no. 8, pp. 1215–1227, Aug. 2006.
- [9] P. Lasaygues, J. P. Lefebvre, and S. Mensah, "High resolution low frequency ultrasonic tomography," *Ultrason. Imaging*, vol. 19, no. 4, pp. 278–293, Oct. 1997.
- [10] M. Loosvelt and P. Lasaygues, "A Wavelet-Based Processing method for simultaneously determining ultrasonic velocity and material thickness," *Ultrasonics*, vol. 51, no. 3, pp. 325–339, Apr. 2011.
- [11] J.-P. Lefebvre, P. Lasaygues, and S. Mensah, "Acoustic Tomography, Ultrasonic

Tomography,” in *Materials and Acoustics Handbook*, M. Bruneau and C. Potel, Eds. London, UK: ISTE, 2009, pp. 887–906.

[12] P. Lasaygues, D. Tanne, S. Mensah, and J. P. Lefebvre, “Circular antenna for breast ultrasonic diffraction tomography,” *Ultrason. Imaging*, vol. 24, no. 3, pp. 177–189, Jul. 2002.

[13] J. P. Lefebvre, P. Lasaygues, S. Mensah, S. Delamare, and A. Wirgin, “Born Ultrasonic Tomography: Some Limits and Improvements,” in *Acoustical Imaging*, vol. 25, M. Halliwell and P. N. T. Wells, Eds. Boston: Kluwer Academic Publishers, 2002, pp. 79–86.

[14] Y. Meyer, “Orthonormal Wavelets,” in *Wavelets*, J.-M. Combes, A. Grossmann, and P. Tchamitchian, Eds. Berlin, Heidelberg: Springer Berlin Heidelberg, 1989, pp. 21–37.

[15] S. Jaffard, Y. Meyer, and R. D. Ryan, *Wavelets: Tools for Science and Technology*. Society for Industrial and Applied Mathematics, 2001.

[16] F. Conil, D. Gibert, and F. Nicollin, “Nonlinear synthesis of input signals in ultrasonic experimental setups,” *J. Acoust. Soc. Am.*, vol. 115, no. 1, p. 246, 2004.

[17] S. Kirkpatrick, C. D. Gelatt, and M. P. Vecchi, “Optimization by Simulated Annealing,” *Science*, vol. 220, no. 4598, pp. 671–680, May 1983.

[18] S. Jaffard, “Construction of Wavelets on Open Sets,” in *Wavelets*, J.-M. Combes, A. Grossmann, and P. Tchamitchian, Eds. Berlin, Heidelberg: Springer Berlin Heidelberg, 1989, pp. 247–252.

[19] R. C. Waag and R. J. Fedewa, “A ring transducer system for medical ultrasound research,” *IEEE Trans. Ultrason. Ferroelectr. Freq. Control*, vol. 53, no. 10, pp. 1707–1718, Oct. 2006.

[20] J. Rouyer, S. Mensah, C. Vasseur, and P. Lasaygues, “The benefits of compression methods in acoustic coherence tomography,” *Ultrason. Imaging*, vol. 37, no. 3, pp. 205–223, Jul. 2015.